WAVES SERIES

METAMATERIALS APPLIED TO WAVES SET

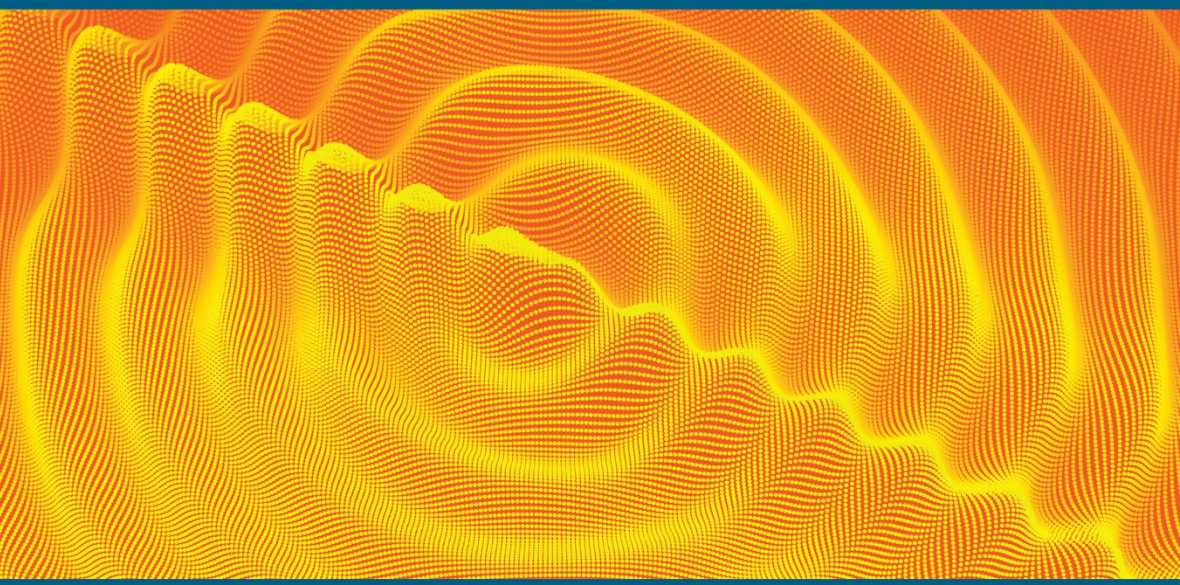

Volume 1

Fundamentals and Applications of Acoustic Metamaterials

From Seismic to Radio Frequency

Edited by
Vicente Romero-García
Anne-Christine Hladky-Hennion

ISTE

WILEY

Fundamentals and Applications of Acoustic Metamaterials

Metamaterials Applied to Waves Set

coordinated by
Frédérique de Fornel and Sébastien Guenneau

Volume 1

Fundamentals and Applications of Acoustic Metamaterials

From Seismic to Radio Frequency

Edited by

Vicente Romero-García
Anne-Christine Hladky-Hennion

ISTE

WILEY

First published 2019 in Great Britain and the United States by ISTE Ltd and John Wiley & Sons, Inc.

ISTE Ltd
27-37 St George's Road
London SW19 4EU
UK

www.iste.co.uk

John Wiley & Sons, Inc.
111 River Street
Hoboken, NJ 07030
USA

www.wiley.com

Library of Congress Control Number: 2019938254

British Library Cataloguing-in-Publication Data
A CIP record for this book is available from the British Library
ISBN 978-1-78630-336-3

Contents

Preface

During recent decades, metamaterials have revolutionized the way waves are controlled in the broad field of wave physics due to the extraordinary physical properties they present. Their locally resonant structure, introducing deep subwavelength band gaps, regions of frequencies where propagation is forbidden, among other properties, have motivated a plethora of applications not available up to now and creating an inflection point in the material science conception. In particular, acoustic metamaterials have shown extraordinary functionalities giving rise to breakthroughs. In many cases, they are able to replace traditional treatments in practical situations due to the better performances in targeted and tunable frequency ranges with strongly reduced dimensions. Acoustic and mechanical metamaterials themselves represent a scientific breakthrough with respect to the conventional treatments for noise, vibrations and radiofrequency problems.

Precursors of such metamaterials are the periodic media. Wave propagation in periodic media has been exploited in the field of wave physics revolutionizing the way of controlling waves in several branches of physics and technology. The secret of these materials lies in their structuring, the origin of peculiar effects like negative refraction or the spatial filtering, explaining, for example, the structural color in nature such as butterfly wings have. Today, these materials count as part of the class of photonic crystals for light or phononic crystals for elastic and acoustic waves with particular dispersion relation. It has been shown that periodic distributions of scatterers embedded in a host medium can be used in the design of effective media in the low frequency regime. When the wavelength, λ, is big compared to the separation between the scatterers, a, (long wavelength regime), homogenization theories can be applied and as a result, this periodic medium behaves as an effective homogeneous medium. If the scatterers are resonators, the effective properties can present extraordinary properties around the resonance frequency, and in this case, the

material becomes a metamaterial. However, in the diffraction regime, the periodic structures present bandgaps at wavelengths of the order of the periodicity of the structure. Among other potential applications, in acoustics these systems have motivated tunable frequency filters, beam forming devices, waveguides, wave traps and slow wave systems. In this regime, these materials are strongly anisotropic, presenting an angular dependence of its scattering properties.

During the summer school *Metagenierie 2017*, organized by the GdR (Groupement de recherche) Meta, the principles of acoustic metamaterials and their possible engineer/industrial applications were discussed with main goal of creating a training course with different steps of the learning procedure: global state of the art, principles and fundamentals and applications. This book is devoted to gathering all the discussions and provides a training book with a large overview on the field of acoustic metamaterials through its nine chapters. The book is divided into three parts:

– Part 1: Overview of the Current Research in Acoustic Metamaterials

– Part 2: Principles and Fundamentals of Acoustic Metamaterials

– Part 3: Applications of Acoustic Metamaterials

Part 1, Chapters 1–3, highlights the properties of the locally resonant structures with deep subwavelength bandgaps, and how the viscothermal losses can affect the physical properties. Chapter 1 shows the recent advances in the study of the presence of losses in double-negative metamaterial; Chapter 2 focuses on the use of deep subwavelength bandgaps to attenuate seismic waves; and finally, Chapter 3 shows how we can make use of both viscothermal losses and slow sound phenomena to create perfect absorbers as well as metadiffusers with deep subwavelength structures.

Part 2, Chapters 4–6, provides the principles and fundamentals of the basic theoretical frameworks to deal with metamaterials and periodic structures. Chapter 4 discusses the homogenization theory for 3D structures in the time domain; Chapter 5 shows the fundamentals of the plane wave expansion method to calculate the dispersion relation of periodic media; and finally, Chapter 6 shows a complete introduction to the multiple scattering theory in order to deal with the finite size effects of periodic structures.

Part 3, Chapters 7–9, shows a broad overview of the industrial applications of metamaterials and periodic media. Chapter 7 shows a review of the acoustic metamaterials for the industrial applications of audible sound; Chapter 8 shows also an extensive review of the possible radiofrequency applications of acoustic metamaterials for radiofrequency applications; and finally, Chapter 9 shows the possibilities of acoustic metamaterials for underwater applications.

The editors of this book would like to acknowledge all the speakers and participants of *Metagenierie 2017*, who have highly enriched scientific discussions. In particular, the editors would like to kindly thank all the participants of this book. They made a great effort and we hope the readers can note this by reading the chapters. We hope that this book will be useful for the community of acoustic metamaterials and motivate future development in this field.

Vicente ROMERO-GARCÍA
Anne-Christine HLADKY-HENNION
May 2019

PART 1

Overview of the Current Research in Acoustic Metamaterials

Fundamentals and Applications of Acoustic Metamaterials: From Seismic to Radio Frequency,
First Edition. Edited by Vicente Romero-García and Anne-Christine Hladky-Hennion.

1

Visco-thermal Effects in Acoustic Metamaterials Based on Local Resonances

1.1. Introduction

Acoustic metamaterials are man-made composite structures whose acoustic properties are new in comparison with that of the components used in their construction. Recent review articles have reported the many fascinating devices based on their extraordinary properties [CUM 16, MA 16, HAB 16]. Among them, acoustic cloaking and negative refraction are phenomena that are currently used to develop devices like noise shelters, acoustic imaging with subwavelength resolution, focusing devices and many others. On the one hand, acoustic cloaking is obtained thanks to the possibility of engineering artificial structures behaving like acoustic materials with an effective anisotropic dynamical mass density [CUM 07, TOR 08]. Later, it was demonstrated that cloaking is also possible with structures with an effective anisotropic bulk modulus, having simultaneously an effective isotropic dynamical mass. On the other hand, negative refraction arises because of the possibility of engineering structures whose effective acoustic parameters (i.e. mass density and bulk modulus) are both negative. Metamaterials with double-negative parameters can be obtained by tailoring structures that have both monopole and dipole resonances [LI 04]. In addition, negative refraction has been also demonstrated using space-coiling acoustic metamaterials [KOC 49, LIA 12, XIE 13] and hyperbolic materials [GAR 14].

The effect of losses in acoustic metamaterials has been scarcely tackled though dissipation seems to play a fundamental role in explaining the degradation of the

Chapter written by José SÁNCHEZ-DEHESA and Vicente CUTANDA HENRÍQUEZ.

predicted performance in many manufactured structures. As a typical example, let us mention the case of three-dimensional labyrinthine acoustic metamaterials characterized by Frenzel *et al.* [FRE 13], who found a significant amount of losses that led them to propose these structures for subwavelength broadband all-angle acoustic absorbers. A recent study by Molerón *et al.* [MOL 16] demonstrated that the actual response of these structures with subwavelength slits in air strongly depends on the viscothermal losses. Previously, it was shown that slow sound propagation observed in waveguides with side resonators was produced by viscothermal dissipation [THE 14]. For the case of metamaterials based on local resonances, the authors claimed the expected double-negative behavior in two specifically designed structures was unobservable, due to the strong influence of viscothermal effects [FOK 11, GRA 13].

This chapter is devoted to study the contribution of viscothermal effects in some specific acoustic metamaterials. Particularly, in those whose negative effective parameters are a consequence of embedded resonances in the building units. First, we briefly report the different approaches developed in order to study viscothermal losses in environments where their expected contribution is relevant. The finite element method (FEM) and the boundary element method (BEM) can be used when explaining the properties of artificial structures with corrugated surfaces where viscothermal losses are relevant, like the ones analyzed here. We have selected the BEM as the more adequate to study the metamaterial samples based on local resonances and therefore we explain this method with some detail in section 1.2.1. Then, in section 1.3, the BEM is applied to comprehensively study the case of a single-negative metamaterial. This quasi-two-dimensional metamaterial structure is made of a two-dimensional (2D) waveguide with a square distribution of drilled holes [GRA 12] and effectively behaves as a material with negative bulk modulus as the one introduced by Fang *et al.* [FAN 06]. It will be shown that the viscothermal losses, although relevant, do not destroy the observation of the negative modulus theoretically predicted. However, this is not the conclusion obtained for the case studied in section 1.4, where the quasi-2D metamaterial has cylindrical inclusions with a periodically corrugated surface and was designed to show double-negative behavior. For this double-negative metamaterial, the viscothermal losses play a paramount importance and its contribution completely destroys the expected behavior, giving support to the experimental data [CUT 17b]. Anyway, we have to stress that the effect of viscothermal losses has been studied for two specific cases and cannot be directly extrapolated to all cases. However, the results are indicative of the type of issues that researchers should consider during the process of designing metamaterials based on embedded resonances.

1.2. Viscothermal effects: numerical methods

Viscous and thermal losses of acoustic waves are only relevant in two cases: i) propagation over long distances, such as large rooms and outdoor acoustics; and ii) a very thin boundary layer of fluid over the domain boundaries. We are not concerned here with case i), which can easily be treated by suitably modifying the existing physical descriptions (e.g. with propagation loss constants). In case ii), viscous and thermal boundary layers have similar thicknesses, ranging from a few micrometers at high frequencies to a fraction of a millimeter at lower frequencies, in the audible range. The viscous and thermal boundary layers arise due to i) the difficulty of the fluid particles to slide over the boundary, and ii) the strong heat exchange between fluid and solid boundary, respectively [PIE 81, MOR 68].

Boundary losses due to viscothermal effects can be accounted for as a boundary impedance in large setups such as rooms [CRE 82]. Such approach is, however, limited for small (in relation to the thickness of the boundary layers) or intricate setups. When the boundary layers fill a significant part, or all, of the volume of the domain, losses can be very relevant. This is the case, for example, of microphones, hearing aids and acoustic couplers. In the case of metamaterials, the effect of viscothermal losses can be very relevant even for cases of a relatively large scale, as will be shown later in this chapter.

Viscothermal losses can be represented by analytical models, such as in the classical solution to a narrow cylindrical tube [RAY 94]. Other authors provide similar solutions, also limited to particular geometries [STI 91, BRU 87]. These solutions are often used in the metamaterial literature. However, their geometrical limitations restrict their range of applicability to simplified versions of quarter-wavelength and Helmholtz resonators.

The BEM with viscothermal losses is used in the test cases shown in the following sections of this chapter. This is a numerical method with no limiting hypotheses other than linearity and absence of flow. The viscothermal implementation of the finite element method (FEM) is another numerical implementation with no geometrical restrictions, which was used in [CUT 17a] to validate BEM metamaterial models. The BEM with losses is chosen here because it has been found more computationally manageable for the metamaterial cases studied.

The FEM and BEM with losses are briefly described in the following sections.

1.2.1. *Finite element method with losses*

The FEM implementation with viscous and thermal losses is available in the commercial software COMSOL. It was initially proposed by Malinen *et al.*

[MAL 04], which is achieved by direct discretization of the full linearized Navier–Stokes equations. The equations solved are the momentum, continuity and energy equations,

$$i\omega\rho_0\mathbf{v} = \nabla\cdot\left(-p\mathbf{I} + \mu\left(\nabla\mathbf{v} + \nabla\mathbf{v}^T\right) - \left(\frac{2}{3}\mu - \eta\right)(\nabla\cdot\mathbf{v})\,\mathbf{I}\right) + \mathbf{F} \qquad [1.1]$$

$$i\omega\rho + \rho_0\nabla\cdot\mathbf{v} = 0 \qquad [1.2]$$

$$i\omega\rho_0 C_p T = -\nabla\cdot(-\lambda\nabla T) + i\omega\alpha_0 T_0 p \qquad [1.3]$$

$$\rho = \rho_0\left(\beta_T p - \alpha_0 T\right) \qquad [1.4]$$

The acoustic variables are: particle velocity $\mathbf{v}$, pressure p and temperature T. $\mathbf{F}$ is a volume force acting on the fluid. The parameters of air are expressed as: ρ_0 the static density, T_0 the equilibrium temperature, μ the coefficient of viscosity, η the bulk viscosity, C_p the heat capacity at constant pressure, λ thermal conductivity, α_0 coefficient of thermal expansion and β_T isothermal compressibility.

Equations [1.1]–[1.4] are solved by transforming the equations into weak form, as is usually done in FEM. This results in a system of equations having pressure, particle velocity and temperature as variables. Five degrees of freedom are introduced per node, meaning that the system will be five times larger as compared to the lossless counterpart for the same mesh. In addition, the boundary layers over the boundaries need to be meshed with sufficient detail, further increasing the size of the calculation.

1.2.2. *Boundary element method with losses*

The BEM implementation with losses is based on the Kirchhoff decomposition of the Navier–Stokes equations [PIE 81, BRU 89],

$$(\Delta + k_a^2)p_a = 0 \qquad [1.5]$$

$$(\Delta + k_h^2)p_h = 0 \qquad [1.6]$$

$$(\Delta + k_v^2)\vec{v}_v = \vec{0}\,,\ \text{with}\ \ \nabla\cdot\vec{v}_v = 0 \qquad [1.7]$$

where harmonic time dependence $e^{i\omega t}$ is omitted. The indexes (*a,h,v*) indicate the so-called acoustic, thermal and viscous *modes*, represented by equations [1.5], [1.6]

and [1.7] respectively. The modes can be treated independently in the acoustic domain and linked through the boundary conditions. The total pressure can be obtained as the sum $p = p_a + p_h$ of the acoustic and thermal components (there is not a viscous pressure), while the particle velocity has contributions from the three *modes* as $\vec{v} = \vec{v}_a + \vec{v}_h + \vec{v}_v$.

$$k_a^2 = \frac{k^2}{1 + ik(\ell_v + [\gamma - 1)\ell_h] - k^2\ell_h(\gamma - 1)(\ell_h - \ell_v)} \quad [1.8]$$

$$k_h^2 = \frac{-ik}{1 - ik(\gamma - 1)(\ell_h - \ell_v)} \quad [1.9]$$

$$k_v^2 = -\frac{i\rho_0 ck}{\mu}, \quad [1.10]$$

The three wavenumbers k_a, k_h and k_v in equations [1.8], [1.9] and [1.10] depend on the lossless wavenumber k and the physical properties of the fluid: ρ_0 is the static density of air, c is the speed of sound, k is the adiabatic wavenumber and γ is the ratio of specific heat at constant pressure and specific heat at constant volume C_p/C_v. The viscous and thermal characteristic lengths are $\ell_v = (\eta + 4/3\mu)/\rho_0 c$ and $\ell_h = \lambda/(\rho_0 c C_p)$, where λ is the thermal conductivity, μ is the coefficient of viscosity and η is the bulk viscosity or second viscosity [BRU 89].

Equation [1.5] is a wave equation, while equations [1.6] and [1.7] are diffusion equations. Equation [1.7] is a vector equation and can be split into its three components, giving a total of five equations with five unknowns: p_a, p_h and the three components of $\vec{v}_v$. The modes in equations [1.5], [1.6] and [1.7] can be linked through the boundary conditions

$$T = T_a + T_h = \tau_a p_a + \tau_h p_h = 0, \quad [1.11]$$

$$\vec{v}_{boundary} = \vec{v}_a + \vec{v}_h + \vec{v}_v = \phi_a \nabla p_a + \phi_h \nabla p_h + \vec{v}_v. \quad [1.12]$$

Equation [1.11] states that the temperature T, with acoustic and thermal components T_a and T_h, remains constant at the boundary, leading to a condition that links the thermal and acoustic pressures p_a and p_h. Equation [1.12] ensures that the total particle velocity, expressed as the sum of acoustic, thermal and viscous contributions, matches the boundary velocity in any direction. The parameters τ_a, τ_h, ϕ_a and ϕ_h depend, like the wavenumbers in equations [1.5], [1.6] and [1.7], on

physical constants and the frequency. The velocity calculation, equation [1.12], is a vector equation, which can be split for convenience into normal and tangential components,

$$\vec{v}_{boundary,n} = \phi_a \frac{\partial p_a}{\partial n} + \phi_h \frac{\partial p_h}{\partial n} + \vec{v}_{v,n}, \qquad [1.13]$$

$$\vec{v}_{boundary,t} = \phi_a \nabla_t p_a + \phi_h \nabla_t p_h + \vec{v}_{v,t}. \qquad [1.14]$$

The BEM implementation with losses starts by discretizing equations [1.5], [1.6] and [1.7] independently. These equations are formally equivalent to the lossless harmonic Helmholtz equation, and therefore the discretization follows the same procedure as in the lossless BEM, i.e. converting the Helmholtz equation into its integral form [WU 00, JUH 93],

$$C(P)p(P) = \int_S \left[\frac{\partial G(Q)}{\partial n} p(Q) - \frac{\partial p(Q)}{\partial n} G(Q) \right] dS + p^I(P), \qquad [1.15]$$

where p is the sound pressure, G is the Green's function, and P and Q are points in the domain and on the surface respectively. $C(P)$ is a geometrical constant and $p^I(P)$ is the incident pressure, if present. The boundary is then divided into surface elements, and equation [1.15] is discretized as

$$\mathbf{A}\mathbf{p} - \mathbf{B}\frac{\partial \mathbf{p}}{\partial n} + \mathbf{p}^I = 0. \qquad [1.16]$$

Given a set of boundary conditions, equation [1.16] can be solved for obtaining the pressure and normal particle velocity at the boundary. The acoustic magnitudes in the domain are subsequently obtained from the surface solution by re-applying the discretized Helmholtz integral equation. By following this procedure, the harmonic equations, equations [1.5], [1.6] and [1.7] of the Kirchhoff decomposition, can be discretized as

$$\mathbf{A}_a\mathbf{p}_a - \mathbf{B}_a\frac{\partial \mathbf{p}_a}{\partial n} + \mathbf{p}^I = 0, \qquad [1.17]$$

$$\mathbf{A}_h\mathbf{p}_h - \mathbf{B}_h\frac{\partial \mathbf{p}_h}{\partial n} = 0, \qquad [1.18]$$

$$\mathbf{A}_v\vec{\mathbf{v}}_v - \mathbf{B}_v\frac{\partial \vec{\mathbf{v}}_v}{\partial n} = \vec{0}\,, \text{ with } \nabla \cdot \vec{\mathbf{v}}_v = 0. \qquad [1.19]$$

The coupling boundary conditions in equations [1.11] and [1.12] and the null divergence of the viscous velocity in equation [1.19] are used in the coupling of equations [1.17], [1.18] and [1.19]. This coupling is better achieved if the velocity

boundary condition is split, as shown in equations [1.13] and [1.14], into components that are locally normal and tangential to the boundary. Coordinate transformations between the node-based local reference system (normal and tangential vectors n, t_1 and t_2) and the global Cartesian reference (x, y, z) are therefore needed. The resulting system of equations for obtaining the acoustic component of the pressure on the boundary is

$$\begin{aligned}
&\Bigg[\phi_a \mathbf{B}_a^{-1}\mathbf{A}_a - \phi_h \mathbf{B}_h^{-1}\mathbf{A}_h \frac{\tau_a}{\tau_h} \\
&+\left[\mathbf{N}_{11} \circ (\mathbf{B}_v^{-1}\mathbf{A}_v)\right]^{-1}\left(\phi_a - \frac{\tau_a}{\tau_h}\phi_h\right)\Bigg(\left[\mathbf{N}_{12} \circ (\mathbf{B}_v^{-1}\mathbf{A}_v)\right]\frac{\partial}{\partial t_1} \\
&+\left[\mathbf{N}_{13} \circ (\mathbf{B}_v^{-1}\mathbf{A}_v)\right]\frac{\partial}{\partial t_2} + \Delta_t\Bigg)\Bigg]\mathbf{p}_a = \\
&\vec{\mathbf{v}}_{boundary,n} + \left[\mathbf{N}_{11} \circ (\mathbf{B}_v^{-1}\mathbf{A}_v)\right]^{-1}\left[\left[\mathbf{N}_{12} \circ (\mathbf{B}_v^{-1}\mathbf{A}_v)\right] + \frac{\partial}{\partial t_1}\right]\vec{\mathbf{v}}_{boundary,t_1} \\
&+\left[\mathbf{N}_{11} \circ (\mathbf{B}_v^{-1}\mathbf{A}_v)\right]^{-1}\left[\left[\mathbf{N}_{13} \circ (\mathbf{B}_v^{-1}\mathbf{A}_v)\right] + \frac{\partial}{\partial t_2}\right]\vec{\mathbf{v}}_{boundary,t_2} - \phi_a \mathbf{B}_a^{-1}\mathbf{p}^I \quad [1.20]
\end{aligned}$$

The "$\circ$" operator in equation [1.20] is the Hadamard matrix product, and the constant matrices $\mathbf{N}_{11}$, $\mathbf{N}_{12}$ and $\mathbf{N}_{13}$ are obtained as

$$\begin{aligned}
\mathbf{N}_{11} &= \mathbf{n}_x\mathbf{n}_x^T + \mathbf{n}_y\mathbf{n}_y^T + \mathbf{n}_z\mathbf{n}_z^T, \\
\mathbf{N}_{12} &= \mathbf{n}_x\mathbf{t}_{1,x}^T + \mathbf{n}_y\mathbf{t}_{1,y}^T + \mathbf{n}_z\mathbf{t}_{1,z}^T, \\
\mathbf{N}_{13} &= \mathbf{n}_x\mathbf{t}_{2,x}^T + \mathbf{n}_y\mathbf{t}_{2,y}^T + \mathbf{n}_z\mathbf{t}_{2,z}^T,
\end{aligned} \quad [1.21]$$

where the right-hand sides contain products of the (x, y, z) components of the node-based normal and tangential vectors n, t_1 and t_2.

Equation [1.20] relates the prescribed normal and tangential velocities on the boundary ($\vec{\mathbf{v}}_{boundary,n}$, $\vec{\mathbf{v}}_{boundary,t_1}$ and $\vec{\mathbf{v}}_{boundary,t_2}$) and the incident pressure $\mathbf{p}^I$ with the boundary pressures associated with the acoustic mode $\mathbf{p}_a$. After solving this system, it is possible to derive the remaining magnitudes on the boundary ($\mathbf{p}_h, \vec{\mathbf{v}}_v$) and on the domain [STI 91, CUT 13].

The implementation is based on the research software OpenBEM, which solves the Helmholtz wave equation using the direct collocation technique [CUT 10]. In BEM, only the domain boundary is meshed, saving degrees of freedom as compared with other numerical methods like the FEM. Three sets of coefficient matrices are used ($\mathbf{A}_a$, $\mathbf{B}_a$, $\mathbf{A}_h$, $\mathbf{B}_h$, $\mathbf{A}_v$, $\mathbf{B}_v$) corresponding to the three modes: acoustic, thermal and

viscous. The thermal and viscous coefficient matrices are, as a result of the evanescent nature of the viscous and thermal effects, sparse matrices. However, the remaining acoustic mode matrix is fully populated, and all of them are frequency dependent. As compared with FEM, the BEM with losses – although still computationally heavy – can be more efficient for intricate geometries that are on the limit of what is achievable, as is the case of the metamaterial examples in this chapter.

New versions of the BEM with losses have been proposed recently that overcome implementation issues arising from the $\frac{\partial}{\partial t_1}$, $\frac{\partial}{\partial t_2}$ and Δ_t operators in equation [1.20] [CUT 18, AND 18]. These operators are the tangential derivatives and the tangential Laplacian respectively.

1.3. Viscothermal effects in metamaterials with negative bulk modulus

The seminal demonstration of a dynamical bulk modulus with negative value was performed by Fang *et al.* [FAN 06], who used a one-dimensional (1D) water channel with an array of Helmholtz resonators.

They found that the measured effective bulk modulus can be fitted to the following frequency-dependent expression:

$$B_{eff}^{-1} = E_o^{-1}\left[1 - \frac{F\omega_0^2}{\omega^2 - \omega_0^2 + i\Gamma\omega}\right], \qquad [1.22]$$

where F is a geometrical factor, ω_0 is the resonant angular frequency of the resonator and Γ is the dissipation loss in the resonating Helmholtz elements. The loss term was determined by a procedure in which the calculated transmission profile was fitted to the transmitted spectral dip, giving a value of $\Gamma = 2\pi \times 400$ Hz. A few years later, an equivalent quasi-two-dimensional structure was studied in airborne sound with similar conclusions [GAR 12]. The structure consisted of a square array of cylindrical boreholes with equal radii (R) and depths (L) drilled in a flat rigid surface. The theoretical profile fitted to the experimental data provided a value for the losses $\Gamma = 2\pi \times 3.4$ Hz. This value is extremely small in comparison with that obtained using an 1D water waveguide with Helmholtz resonators.

To verify such small amount of losses, we have performed numerical simulations using the BEM implementation described above. The boundary mesh is constructed using the Gmsh meshing software [GEU 09]. The quadratic six-node elements are represented in Figure 1.1. The dimensions of the structure correspond to what was studied in [GAR 12]. The distance between vertical holes (lattice constant) is 30 cm. They are drilled in an infinite 2D waveguide, which is assumed to carry an incident plane wave. This condition is reproduced in the finite structure shown in Figure 1.1 by

placing a moving piston on the emitting end. In addition, a boundary impedance of ρc is defined at both emitting and receiving ends.

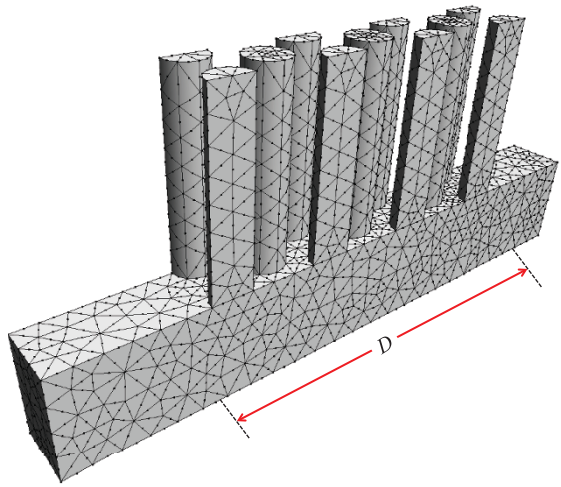

Figure 1.1. *Schematic view of the modeling of an acoustic metamaterial with effective bulk modulus negative. The BEM mesh used consists of 2352 elements and contains 4706 nodes*

Following the experimental setup, reflectance and transmittance are calculated from the acoustic pressures (P_1, P_2, P_3) recorded at three different positions (x_1, x_2, x_3) inside the waveguide; two at the emitting end, in front of the sample, and one at the receiving end, behind the sample. The positions are, respectively, –15.07 cm, –13.9 cm and 15.07 cm, measured from the sample center. The expressions for the reflection and transmission coefficients are:

$$r(\omega) = \frac{P_2 e^{-ik_0 x_1} - P_1 e^{-ik_0 x_2}}{P_1 e^{ik_0 x_2} - P_2 e^{ik_0 x_1}}, \qquad [1.23]$$

$$t(\omega) = \frac{P_3}{P_2} \frac{e^{-ik_0 x_2} - r(\omega) e^{ik_0 x_2}}{e^{-ik_0 x_3}} e^{-ik_0 D}, \qquad [1.24]$$

where k_0 is the wavenumber in air and D is the effective thickness of the metamaterial, which has been determined by considering that the surfaces are located at a half of the distance of the layer separation. From the expressions above, it is possible to obtain the reflectance $R(\omega) = |r(\omega)|^2$ and transmittance $T(\omega) = |t(\omega)|^2$. In addition, the energy balance can be applied to obtain the absorptance $A(\omega) = 1 - T(\omega) - R(\omega)$.

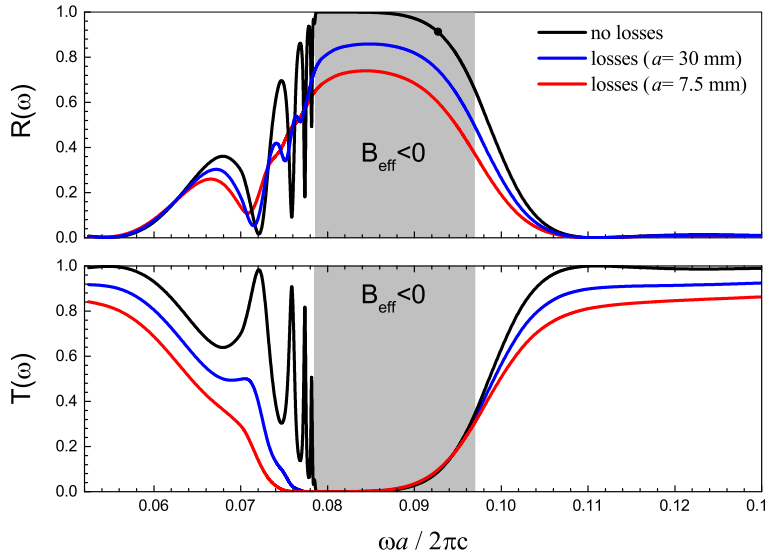

Figure 1.2. *Reflectance $R(\omega)$ and transmittance $T(\omega)$ of the single-negative acoustic metamaterial shown in Figure 1.1. The curves correspond to calculations with no viscothermal losses (black line), and with losses at two different scales: full (blue line) and reduced to one-fourth (red line). The frequencies are given in reduced units to represent all the spectra in a single plot. For a color version of this figure, see www.iste.co.uk/romero/metamaterials.zip*

Figures 1.2 and 1.3 show the reflectance, transmittance and absorptance spectra calculated for the single-negative metamaterial under study. The calculations have been performed with no losses and with viscothermal losses, the latter at two different scales: full and reduced to one-fourth. The reasoning behind the scaling is that viscous and thermal losses do not scale in the same way as the lossless magnitudes. The absorptance for the structure without losses is not shown in Figure 1.3; its value is zero, with the precision of the calculation for all the frequencies, proving that the balance of energy is correct in the calculations. The behavior of the lossless structures does not change with the scale; the results are just shifted in frequency. However, viscous and thermal boundary layers, as mentioned in section 1.2, have thicknesses that vary as $f^{-\frac{1}{2}}$.

Results in Figure 1.2 support the previous simulations, based on the mode-matching technique and the measured data reported in [GAR 12] (see its Figure 1.4). Thus, the calculated spectra with no losses exhibit Fabry–Perot (FP)

peaks (in the transmittance) and troughs (in the reflectance), which are a result of the finite thickness of the metamaterial. Then, a stop band develops in the frequency region (gray strip) where the effective bulk modulus takes negative values and, therefore, the phase velocity is imaginary. When losses are considered, our calculation shows that the FP peaks in the transmittance were strongly reduced and even disappeared when they were experimentally observed. Similar behavior is observed in the reflectance spectra, where the minima defining the FP resonances practically disappear; only the first minimum is kept at both structures. Both the reflectance and transmittance calculated profiles reproduce fairly well the experimental data shown in Figure 4 of [GAR 12], corresponding to the larger dimension. The reason explaining the strong reduction in the transmittance as the frequency is approaching to the bandgap is the corresponding decreasing of the group velocity, which produces an enhancement of the relatively small viscothermal losses.

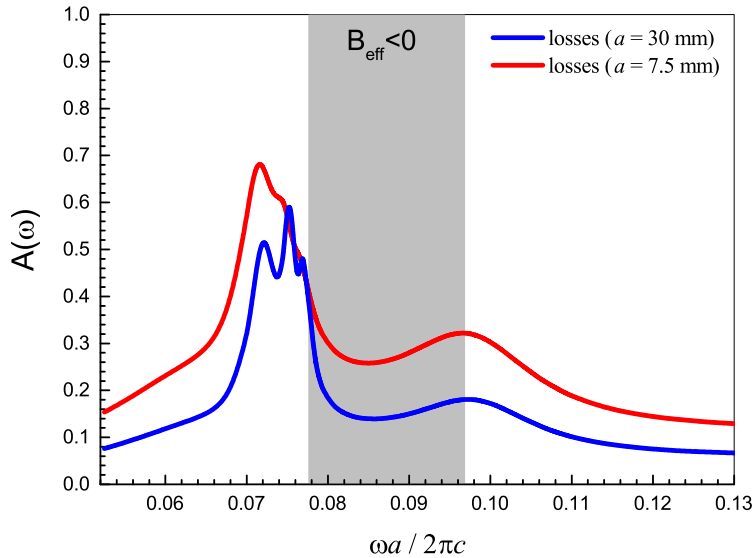

Figure 1.3. *Calculated spectra for the absorptance, $A(\omega)$, of the metamaterial shown in Figure 1.1. Both curves correspond to calculations with viscothermal losses but using structures with two different dimensions. Results obtained with the lattice period $a = 30$ cm (blue line) correspond to the sample studied in [GAR 12], while results obtained with $a = 7.5$ cm (red line) correspond to a scaled-down structure to one-fourth of the original dimensions. Frequencies are given in reduced units to represent both spectra in one plot. For a color version of this figure, see www.iste.co.uk/romero/metamaterials.zip*

It is shown in Figure 1.3 that the absorptance has two maxima: one in the region where the FP resonances are excited and another, located at about 0.096 reduced units, where the imaginary component of the effective modulus has a maximum. Thus, for this single-negative metamaterial, we can conclude that losses due to FP resonances are more efficient in dissipating the incoming energy than that produced by the monopole resonances that provoke the negative bulk modulus. This is not the case for the double-negative structures as explained in section 1.4.

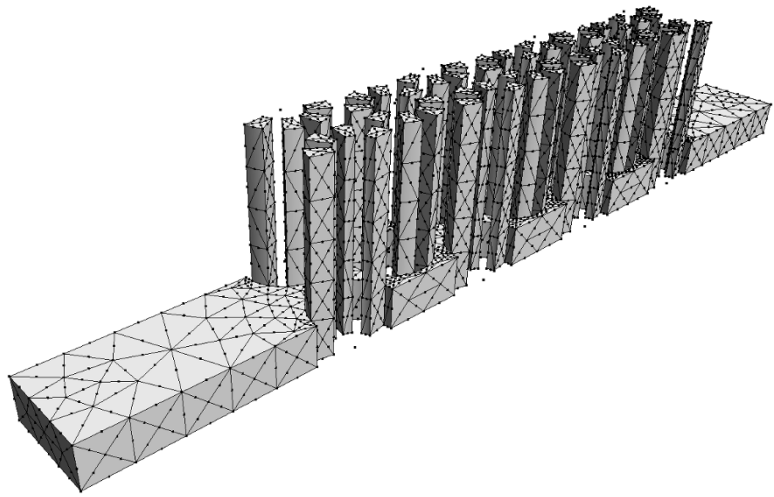

Figure 1.4. *Schematic view of the structure studied in [GRA 13] as an acoustic metamaterial with double-negative parameters. The BEM mesh consists of 4810 elements and contains 9616 nodes*

Regarding the dissipation loss Γ in the resonant elements, we have followed the standard described in previous works [FAN 06, GAR 12]. When no losses are considered, the fitting of B_{eff} obtained from our BEM simulations to the profile in equation [1.22] gives $\Gamma \approx 2\pi \times 0.022$. This value is smaller than confidence bounds and therefore it can be considered zero within the numerical tolerance of the BEM algorithm, as can be expected from the physical description. When losses are considered, $\Gamma \approx 2\pi \times 15.6$, for the full structure, it indicates that our simulation overestimated in about an order of magnitude the experimental data. For the structure scaled down to one-fourth, $\Gamma \approx 2\pi \times 127.3$, about an order of magnitude larger. This last result might lead to the conclusion that losses can be mitigated in metamaterials by using samples with larger dimensions. As we will discuss below, this is not the